Fracture Mechanics of Concrete and Concrete Structures -
High Performance, Fiber Reinforced Concrete, Special Loadings and Structural Applications- B. H. Oh, et al. (eds)
 ISBN 978-89-5708-182-2

# Variations in cracking resistance of self-consolidating concrete at early age

S.H. Kwon, K. Choi, S.D. Cho & H.Y. Park
*Myongji University, Yongin, South Korea*

ABSTRACT: This study investigated experimentally and analytically changes in the cracking resistance of self-consolidating concrete at an early age. Wedge-splitting tests were performed with four different SCC mixes at 1, 2, 3, 14, and 28 days. Softening curves that optimally fit the measure load-CMOD curves were found by inverse analysis. Using the results of the tests and inverse analyses, we examined how fracture energy and four parameters of bilinear softening curves vary at early ages, and on this basis we suggest a model for determining the effects of age on the softening curve.

## 1 INTRODUCTION

Self-Consolidating Concrete (SCC) has seen increasingly widespread usage worldwide by virtue of its numerous attractive features such as low construction cost, high-quality finish, and easy and high-speed casting with little labor. SCC has been quite successfully established in the precast industry, and is now increasingly used in cast-in-place concrete construction (Benedict 2005).

The shortcomings of SCC are mainly related to its fresh state; for example, robustness, high formwork pressure and test methods to ensure its flowability and compactibility (Lange 2007). Much research has been performed to resolve these shortcomings, but research on SCC's mechanical properties has been relatively limited. Typically with SCC, binder content is very high, a small size aggregate is used, and much chemical and pozzolanic admixtures are added to the mix. Therefore, mechanical properties, especially variations in the properties at an early age may be quite different from those of ordinary concrete.

The fundamental vulnerability of concrete is tensile cracking, which is one of the most important properties that need to be examined. In this study, the variations in the tensile fracture properties at an early age was investigated. Wedge-splitting tests for four different SCC mixes were carried out at 1, 2, 3, 7, 14, and 28 days. The strain softening curve that optimally fit the load-CMOD curve of each specimen was found through inverse analysis. Based on the test and analysis results, this study examined how the fracture energy and parameters of the softening curves vary as the age increases. A model for the softening curve at an early age is also suggested.

## 2 EXPERIMENTS

### 2.1 *Materials*

Table 1 shows the mix proportions of four SCC mixes. The water-to-binder ratio ranged from 0.31 to 0.37, type I cement was used in all the mixes, and a viscosity modifying agent (VMA) was added to prevent segregation. The maximum aggregate size was 9mm.

The flowability of the mixes was examined from the slump flow test right after mixing. The flow diameter ranged from 620 to 700 mm, and the T50 time was 4.5 to 5.0 seconds in every mix. The mixes satisfied the general requirement for flowability of self-consolidating concrete (Ferrara et al. 2007).

Table 1. Mix proportions.

| Mix | w/b % | Unit mass(kg/m$^3$) | | | | | | |
|---|---|---|---|---|---|---|---|---|
| | | Binder | | W | S | G | SP | VMA |
| | | C | F.A. | | | | | |
| SCC1 | 37 | 417 | 146 | 209 | 859 | 756 | 3.38 | 3.38 |
| SCC2 | 35 | 455 | 136 | 208 | 834 | 751 | 3.55 | 3.55 |
| SCC3 | 33 | 499 | 125 | 207 | 810 | 745 | 3.74 | 3.74 |
| SCC4 | 31 | 545 | 109 | 205 | 787 | 740 | 3.92 | 3.92 |

### 2.2 *Specimens and test setup*

Twelve specimens were manufactured with each SCC mix for the wedge-splitting tests. The specimens were wrapped with a wet curing blanket and kept in a constant temperature room at 20℃ right after casting.

Figure 1 shows the dimensions of the specimens and test setup for the wedge-splitting tests. Two companion specimens were tested at 1, 2, 3, 7, 14, and 28 days. The tests were conducted with a servo-hydraulic closed-loop testing machine. The applied load was measured by a 100kN capacity load cell, and the crack mouth opening displacement (CMOD) was measured with a clip-on gage of 5mm capacity. The actuator was controlled by a constant CMOD rate of 0.02 mm/min.

The compressive strength tests were also performed at the same ages as the wedge-splitting tests.

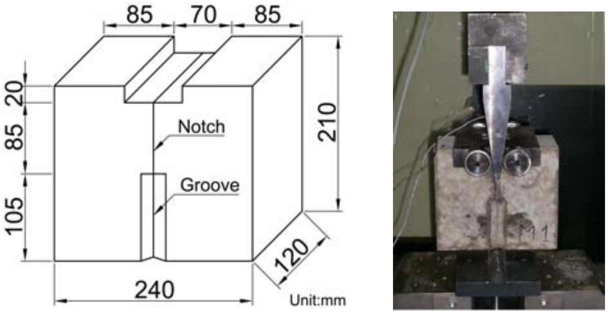


Figure 1. Specimen dimensions and wedge-splitting test setup.

## 3 INVERSE ANALYSIS

### 3.1 *Data processing for companion specimens*

The test data measured from two companion specimens were averaged in the method proposed by a previous study (Zhao et al. 2008). There are several data processing steps in the averaging method. First, the data scattered far from the load-CMOD curve are filtered, and one point is taken every 20 points along the load-CMOD curve (Fig. 2(a)). Second, an average is taken of five points consisting of the given point in the first step and two points above and below the given point. Third, 100 equally spaced CMOD values are calculated from the zero point to the CMOD at the peak load point, and another 100 CMOD values are calculated from the peak to the end point. The end point of the CMOD for each specimen is set such that the distance from the peak to the end point is identical for the two companion specimens. Fourth, the load values corresponding to the 100 CMOD values are calculated by interpolation between the averaged data points for the ascending and descending parts (Fig. 2(b)). Finally, the 200 CMOD values and the corresponding load values for each companion are averaged in the order sequenced (Fig. 2(c)).

### 3.2 *Inverse analysis*

In order to find the softening curve that optimally fits the load-CMOD curves measured at different ages, an inverse analysis was conducted. Because the number of data points used in the optimal fit of the inverse analysis significantly affects computer running time, the minimum number of data points representing the load-CMOD curve is desirable. From the averaged data for the companion specimens, the minimum number of data points were extracted according to the method proposed in the previous study. Six points and twelve points were found for the ascending and descending parts, respectively (Fig. 2(d)).

In the inverse analysis, the strain softening curve was assumed to be bilinear as shown in Figure 3. Figure 4 shows the algorithm of the inverse analysis, in which finite element analysis is repeatedly performed, altering the parameters of the softening curve until the error between the measured and calculated load-CMOD curves is less than a given tolerance (Kwon et al. 2008). Figure 5 is the finite element mesh refinement for the wedge-splitting specimen. Only half of the specimen was modeled considering its symmetry The total number of elements and the number of nodes on the ligament were 596 and 35, respectively.

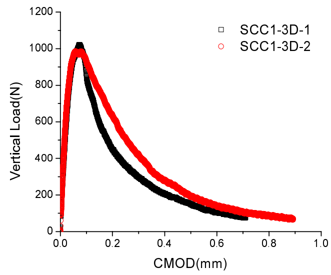


(a) Raw data

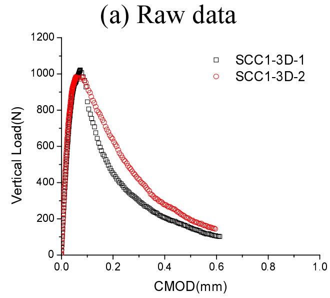


(b) 200 points in each companion

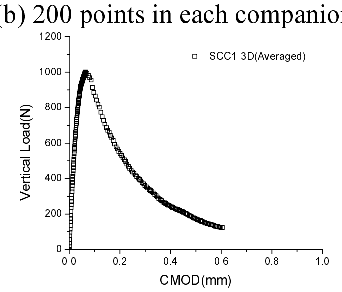


(c) Averaged load-CMOD

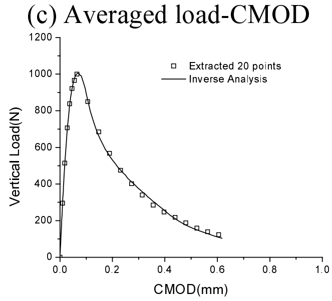


(d) Extracted 20 points and curve fit

Figure 3. Data processing for companion specimens.

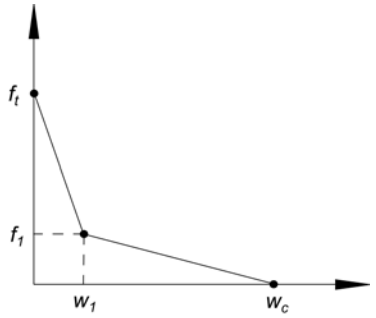


Figure 3. Bilinear softening curve.

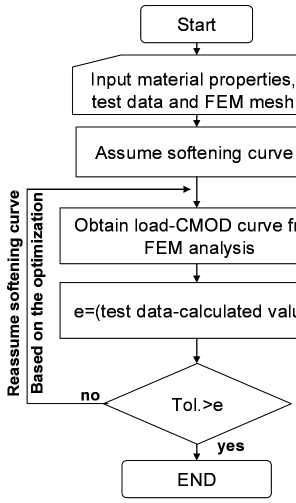


Figure 4. Algorithm of inverse analysis.

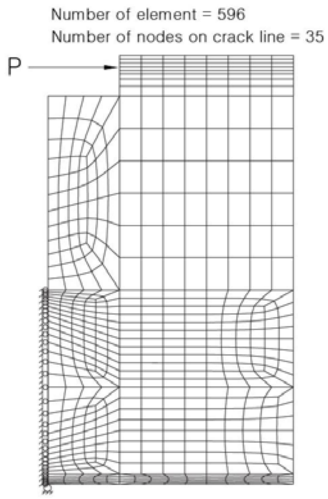


Figure 5. Finite element mesh.

# 4 RESULTS

## 4.1 *Test and inverse analysis results*

The parameters of the bilinear softening curve obtained from the inverse analysis and the measured compressive strength are listed in Table 2. The elastic modulus used as the input of the inverse analysis were calculated based on the compressive strength using the following equation, which is the initial tangent modulus suggested in CEB-FIP model code 1990 (CEB 1993):

$$E_c(t) = 2.15 \times 10^4 \left[ \frac{f_c(t)}{10} \right]^{\frac{1}{3}} \tag{1}$$

In Equation (1), $E_c(t)$ is the elastic modulus, $f_c(t)$ is the compressive strength, and $t$ is the concrete age.

Figure 6 is the comparison between the measured load-CMOD and the load-CMOD calculated based on the optimized softening curve. The calculated load accurately simulates the real load-CMOD curve.

Table 2. Parameters of softening curves and compressive strength.

| Mix | Age | 4 Parameters of Softening Curves | | | | Compressive Strength (MPa) |
|---|---|---|---|---|---|---|
| | | $f_t$ MPa | $f_1$ MPa | $w_1$ mm | $w_c$ mm | |
| SCC1 | 1D | 2.06 | 0.39 | 0.017 | 0.168 | 21.6 |
| | 2D | 3.16 | 0.56 | 0.020 | 0.132 | 33.4 |
| | 3D | 3.20 | 0.91 | 0.018 | 0.099 | 35.9 |
| | 7D | 3.79 | 0.55 | 0.022 | 0.162 | 46.6 |
| | 14 | 4.08 | 0.83 | 0.022 | 0.144 | 50.3 |
| | 28 | 4.94 | 1.07 | 0.014 | 0.096 | 54.4 |
| SCC2 | 1D | 2.68 | 0.49 | 0.020 | 0.160 | 27.3 |
| | 2D | 4.20 | 0.87 | 0.013 | 0.085 | 38.4 |
| | 3D | 4.23 | 0.77 | 0.016 | 0.095 | 40.3 |
| | 7D | 4.48 | 0.93 | 0.018 | 0.105 | 52.8 |
| | 14 | 4.93 | 1.46 | 0.010 | 0.070 | 55.8 |
| | 28 | 5.02 | 1.10 | 0.016 | 0.093 | 55.8 |
| SCC3 | 1D | 3.39 | 1.12 | 0.010 | 0.085 | 34.5 |
| | 2D | 3.86 | 0.89 | 0.018 | 0.105 | 41.9 |
| | 3D | 3.92 | 0.92 | 0.020 | 0.103 | 44.9 |
| | 7D | 3.91 | 0.88 | 0.022 | 0.095 | 47.7 |
| | 14 | 4.54 | 0.82 | 0.019 | 0.069 | 53.0 |
| | 28 | 4.99 | 0.95 | 0.016 | 0.083 | 53.5 |
| SCC4 | 1D | 3.12 | 0.58 | 0.021 | 0.146 | 36.9 |
| | 2D | 3.58 | 0.78 | 0.019 | 0.104 | 43.3 |
| | 3D | 3.77 | 0.87 | 0.016 | 0.118 | 45.5 |
| | 7D | 4.01 | 0.79 | 0.021 | 0.113 | 49.2 |
| | 14 | 4.12 | 0.55 | 0.020 | 0.139 | 62.3 |
| | 28 | 4.19 | 0.79 | 0.022 | 0.105 | 64.9 |

The compressive strengths at different ages were divided by the strength at 28 days, and the normalized values were fitted with the following equation, which is suggested in CEB-FIP model code 1990 (CEB 1993):

$$\beta_{cc}(t) = \exp\left\{ s \left[ 1 - \left( \frac{28}{t} \right) \right]^{1/2} \right\} \tag{2}$$

In Equation (2), $\beta_{cc}(t)$ is the function representing the evolution of strength over time. The parameter $s$ was determined by fitting the normalized values as shown in Figure 7, and its value is 0.145.

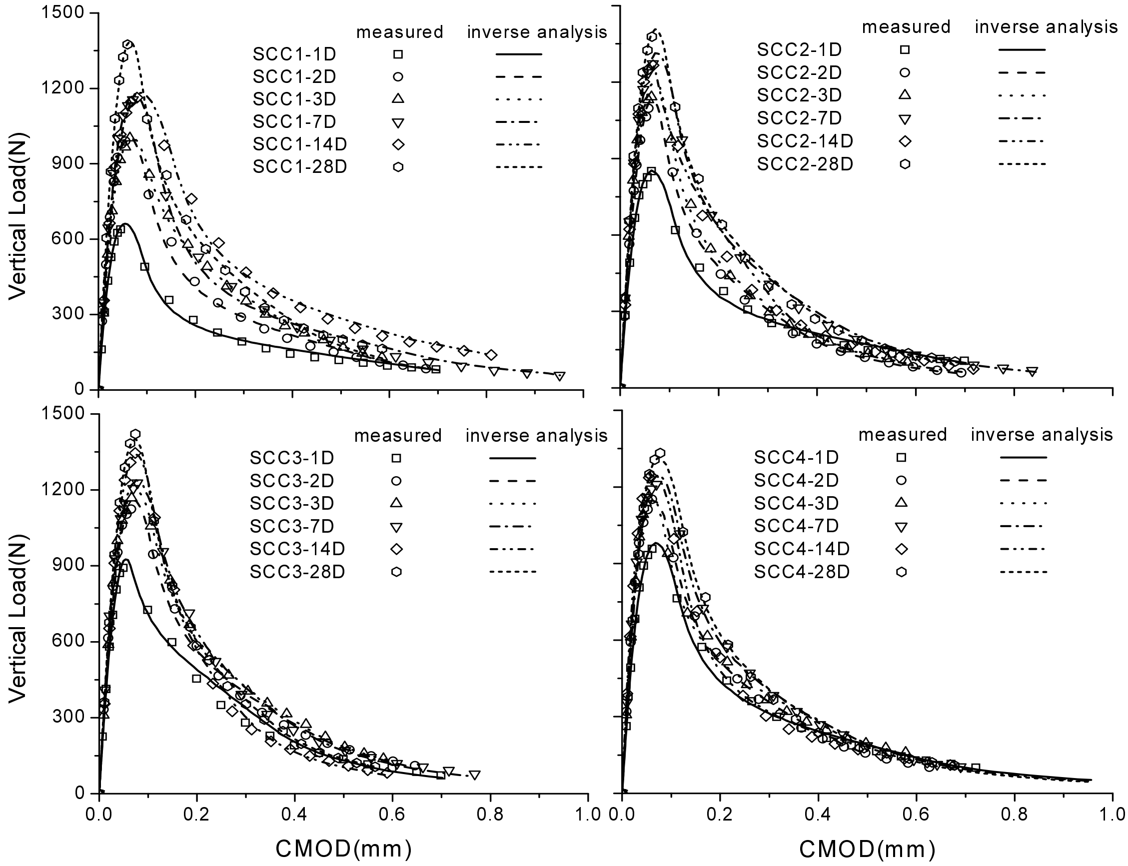

Figure 6. Comparison between the measured load-CMOD curves and the curve fit results.

The fracture energy $G_F$ can be obtained by calculating the area under the softening curve as shown in Figure 8. The fracture energy also increases as the age increases, and is fitted by using the following equation suggested in CEB-FIP 1990 model (CEB 1993).

$$G_F = G_{F0}\left(\frac{f_c(t)}{10}\right)^{\alpha} \tag{3}$$

In Equation (3), $G_{F0}$ and $\alpha$ are constant, and the compressive strength $f_c(t)$ can be obtained by multiplying the compressive strength at 28 days with Equation (2). Figure 9(a) shows the normalized fracture energy with the fracture energy at 28 days and the curve fit results. The determined values of $G_{F0}$ and $\alpha$ are 0.0379 and 0.484, respectively.

The fracture energy is the sum of the area under the first branch of the softening curve and the area under the second branch as shown in Figure 8. The former is $G_{F1}(t)$ and the latter $G_{F2}(t)$ were normalized with the fracture energy or the total area $G_F(t)$ and are plotted in Figures 9(b) and (c). The normalized $G_{F1}(t)$ increases at the beginning and then gradually approaches a certain value. In order to model this time-varying feature of $G_{F1}$, the following equation was fitted with the data of Figure 9(b):

$$r_{G1} = \frac{G_{F1}(t)}{G_F(t)} = \gamma + \frac{\eta(t-1)}{\delta + (t-1)} \tag{4}$$

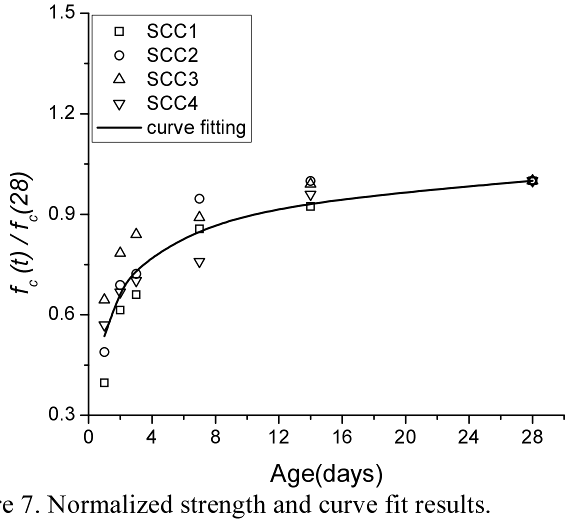

Figure 7. Normalized strength and curve fit results.

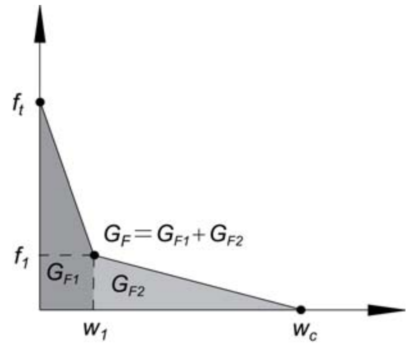


Figure 8. Fracture energy.

In Equation (4), $r_{G1}$ is the normalized $G_{F1}$, and $G_F(t)$ is the fracture energy at age $t$. The values of the constants $\gamma$, $\eta$, and $\delta$ determined by the curve fit are 0.436, 0.135, and 0.551, respectively. The function $r_{G2}$ is defined as follows, and the sum of $r_{G1}$ and $r_{G2}$ is one.

$$r_{G2} = \frac{G_{F2}(t)}{G_F(t)} \qquad r_{G2} + r_{G2} = 1.0 \tag{5}$$

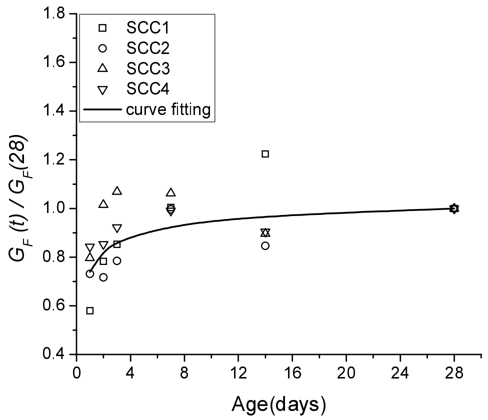


(a) Fracture energy

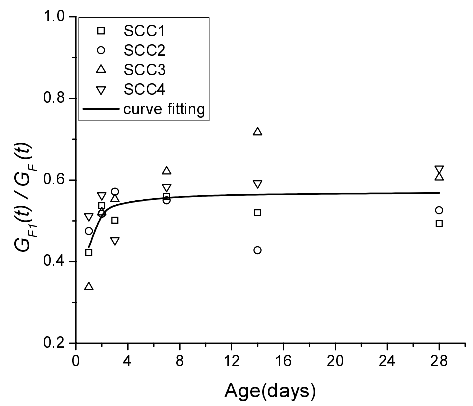


(b) Fracture energy under first branch of softening curve

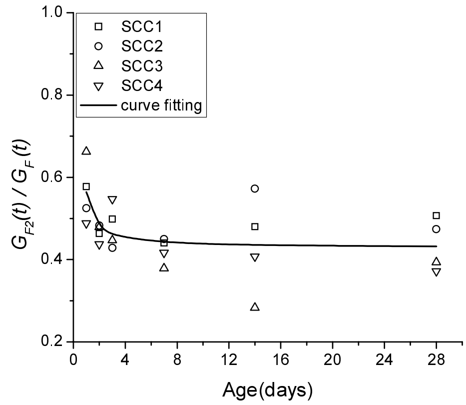


(c) Fracture energy under second branch of softening curve

Figure 9. Normalized fracture energy and curve fit result.

As shown in Figure 9(c), the function $r_{G2}$ steeply decreases at the beginning and asymptotically reaches a certain value in the contrary to the function $r_{G21}$.

Mihashi et al. have suggested a correlation between the softening curve and the mechanism of the fracture process zone (Nomura et al. 1991). According to their study, micro cracks start to grow immediately before the stress reaches the tensile strength. After reaching the tensile strength, the micro cracks are localized and extended along a potential line of macro cracks. The first branch of the softening curve corresponds to the localization and the extension of the micro cracks. Even after the separation of the crack surface, stress can be transmitted by the bridging effect of the coarse aggregates across the main crack. This bridging stress corresponds to the second branch of the softening curve.

Based on the results of Figures 9(b) and (c), it was found that the proportion of energy needed for formation, localization and extension of micro cracks in total fracture energy increased as the age increased, and the proportion of energy consumed by the bridging effect decreased. This feature on variation of the fracture energy over time will be considered in a model for the aging effect of the softening curve suggested in the subsequent section.

### 4.2 *Effect of age on the softening curve*

In Table 2, the two parameters, $f_t$ and $w_c$, show a relatively definite trend over time compared to other parameters, $f_1$ and $w_1$ ; that is, $f_t$ increases and $w_c$ decreases as the age increases.

The parameter $f_t$ was fitted by using the following equation suggested in CEB-FIP model code 1990 (CEB 1993):

$$f_t(t) = f_{t0}\left(\frac{f_c(t)}{10}\right)^{\beta} \tag{6}$$

In Equation (6), $f_{t0}$ and $\beta$ are constant, and the compressive strength $f_c(t)$ can be obtained by multiplying the compressive strength at 28 days with Equation (2). The determined values of $f_{t0}$ and $\beta$ are 1.30 and 0.739, respectively. Figure 10 shows the normalized $f_t$ and curve fit result.

The parameter $w_c$ was also fitted with the following equation suggested in the CEB-FIP 1990 model (CEB 1993):

$$w_c(t) = \mu \frac{G_F(t)}{f_t(t)} \tag{7}$$

In Equation (7), $G_F(t)$ and $f_t(t)$ can be obtained from Equations (3) and (6), respectively. The values of $w_c$ were averaged for all the mixes according to their respective ages, and the function $w_c(t)$ was fitted with the averaged values based on the averaged compressive strength at 28 days; that is, $G_F(t)$ and $f_t(t)$ were calculated based on the compressive strength at 28 days averaged for all the mixes. The constant $\mu$ determined from the curve fitting was 5.57.

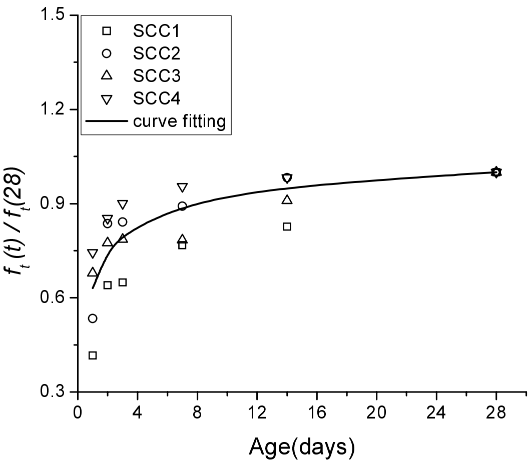


Figure 10. Normalized $f_t$ and curve fit result.

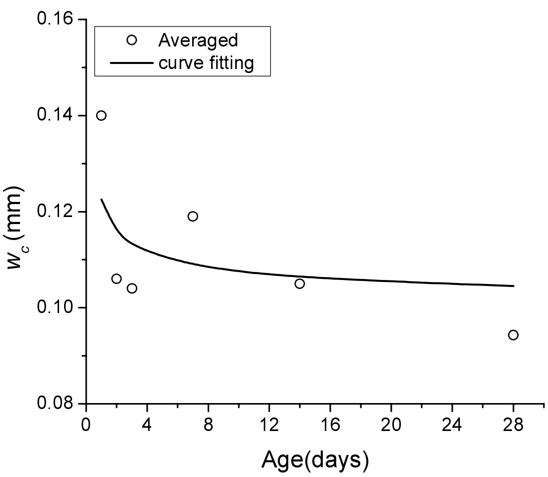


Figure 10. Averaged $w_c$ and curve fit result.

4.3 *A model for the aging effect of the softening curve of self-consolidating concrete*

Based on the test and inverse analysis results, the compressive strength, fracture energy, $f_t(t)$, and $w_c(t)$ were fitted with the corresponding equations suggested in CEB-FIP model code 1990 (CEB 1993). If the two parameters $f_1$ and $w_1$ are determined, then a model for the aging effect of the softening curve can be made. The energy $G_{F1}(t)$ and $G_{F2}(t)$, which correspond to the areas under the first branch and second branch of the softening curve, respectively, can be expressed by the following equations:

$$G_{F1}(t) = r_{G1}(t)G_F(t) = \frac{1}{2} w_1(t)\left[f_t(t) + f_1(t)\right] \tag{8}$$

$$G_{F2}(t) = r_{G2}(t)G_F(t) = \frac{1}{2} f_1(t)\left[w_c(t) - w_1(t)\right] \tag{9}$$

In Equations (8) and (9), $r_{G1}(t)$ and $r_{G2}(t)$ can be calculated from Eqs. (4) and (5), $G_F(t)$ from Equation (3), and $f_t(t)$ and $w_c(t)$ from Equations (6) and (7), respectively. Now, Equations (8) and (9) form a system of quadratic equations with the two variables, $f_1(t)$ and $w_1(t)$, which can be solved by the following:

$$w_1 = \frac{2G_{F1}}{f_t + f_1} \tag{10}$$

$$w_c f_1^2 + \left[w_c f_t - 2G_{F1} - 2G_{F2}\right] f_1 - 2G_{F2} f_t = 0 \tag{11}$$

In Eqs. (10) and (11), the parameter $t$ representing the concrete age is omitted. The four parameters of the softening curve can be calculated from Eqs. (6), (7), (10), and (11), and these equations can be used as a model to present the effect of ages on the softening curve of self-consolidating concrete.

Figure 11 shows the comparison between the parameters of the inverse analysis and the parameters calculated from the model. Although there are deviations between the model and the inverse analysis results, it can be seen that the model has the same trend on the variation of the parameters over ages as that of the inverse analysis results.

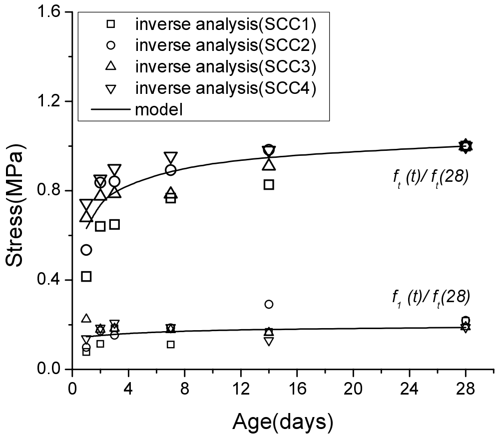


(a) The parameters $f_t(t)$ and $f_1(t)$ of the softening curve

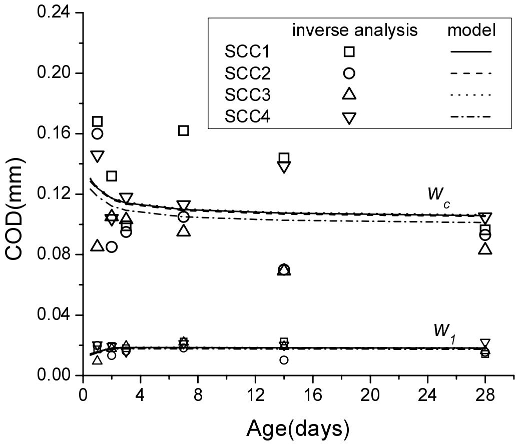


(b) The parameters, $w_c(t)$and $w_1(t)$, of the softening curve

Figure 11. Comparison between the inverse analysis result and the model for aging effect of the softening curve.

In order to examine how much load-CMOD calculated from the model deviates from the measured load-CMOD curve, peak loads and CMOD at peak load were compared in Figures 12 and 13, respectively. In Figures 12(a) and 13(a), the optimized softening curve gives very close peak loads and CMODs to the measured ones. As shown in Figures 12(b) and 13(b), although the peak loads and CMODs calculated based on the model deviate more to the 45-degree inclined line compared to those based on the optimized softening curve, the deviation is still small enough to predict the real peak loads and CMODs at peak loads by the model.

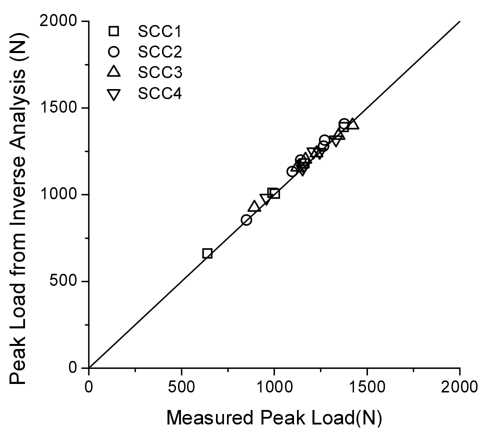


(a) Measured peak loads and peak loads calculated based on the optimized softening curve

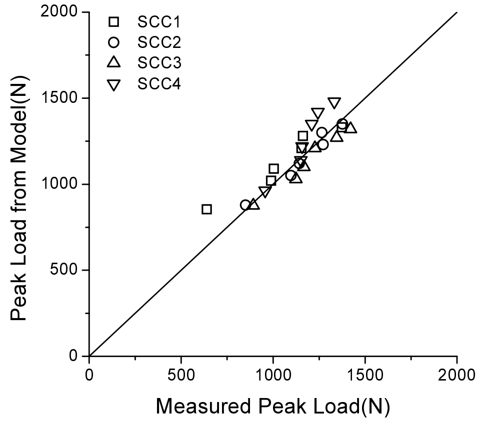


(b) Measured peak loads and peak loads calculated based on the models for the aging effect of the softening curve

Figure 12. Comparison for peak loads.

As mentioned previously, the fracture energy is the area under the softening curve as shown in Figure 8. The fracture energies were calculated from the optimized softening curve and the model, respectively, and were compared in Figure 14. Although the deviation is larger than those shown in Figures 12 and 13, the data points are symmetrically distributed and gather near the 45-degree inclined line. The averaged difference between the fracture energies obtained from the inverse analysis and the model is 0.00624 N/mm. This amount of difference is small enough to predict real tensile fracture behavior by the model.

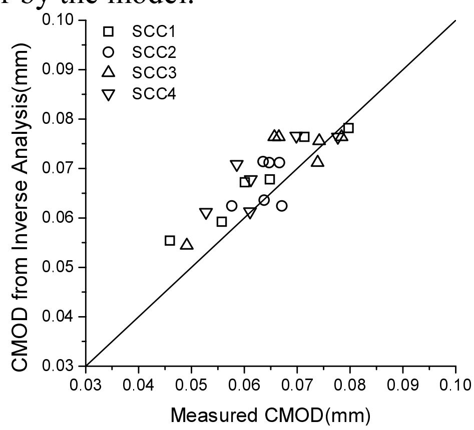


(a) Measured CMODs at peak loads and CMODs at peak loads calculated based on the optimized softening curve

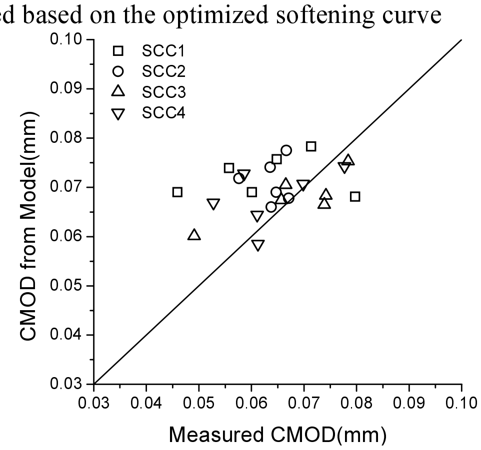


(b) Measured CMODs at peak loads and CMODs at peak loads calculated based on the optimized softening curve

Figure 13. Comparison for CMODs at peak loads

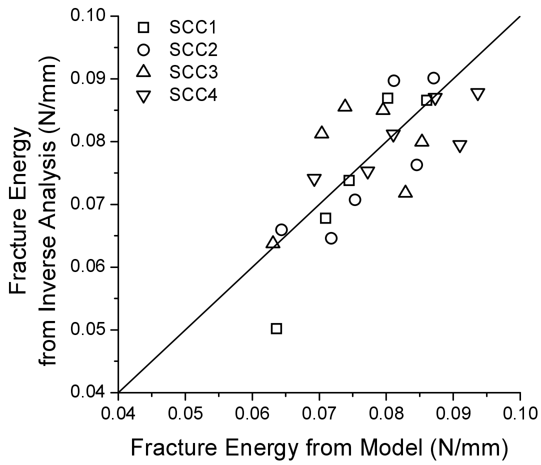


Figure 14. Comparison between fracture energies calculated from the optimized softening curve and the model.

## 5 CONCLUSION

In order to investigate changes in the tensile cracking resistance of self-consolidating concrete at an early age, wedge-splitting tests were performed with four different SCC mixes at different ages, and inverse analyses were carried out to find strain softening curves that optimally fit the load-CMOD curves measured in the tests. From the experiments and the analyses, it was found that the fracture energy increases with age. In particular, the proportion of energy corresponding to the area under the first branch of the softening curve to the total fracture energy increases as the age increases. This means that the proportion of energy needed for the formation, localization, and extension of micro cracks grows larger than the proportion of the energy related to the bridging effect over time. Considering this finding on the fracture energy and the optimal fits for the tensile strength and maximum crack opening displacement, a model for the effect of aging on the softening curve of self-consolidating concrete was suggested. The model gives the four parameters of softening curves varying over ages, and can be used to predict tensile fracture behavior without a large amount of error.

## 6 ACKNOWLEDGMENTS

This work was supported by the Korea Research Foundation Grant funded by the Korean Government (MOEHRD, Basic Research Promotion Fund) (KRF-2008-331-D00596).

## REFERENCES

Benedict, D. E. 2005. Economically attractive field applications for self-consolidating concrete. In Surendra P. Shah (ed.), SCC 2005; The Second North American Conference on the Design and Use of Self-Consolidating Concrete (SCC) and the Fourth International RILEM Symposium on Self-Consolidating Concrete; Proc. Intern. Conf. Chicago, November 2005.:1055-1060. A Hanley Wood Publication.

Comité Euro-International du Béton. 1993. CEB-FIP Model Code 1990: Thomas Telford.

Ferrara, L., Park, Y. D. & Shah, S. P. 2007. Cracking of fiber-reinforced self-compacting concrete due to restrained shrinkage. Cement and Concrete Research 37(6): 957-971.

Kwon, S. H., Zhao, Z. & Shah, S. P. 2008. Effect of specimen size on fracture energy and softening curve of concrete: Part II. Inverse analysis and softening curve. Cement and Concrete Research 38(8-9): 1061-1069.

Lange, D.A. 2007. Self-Consolidating Concrete: A white paper by researchers at the center for advanced cement-based materials. ACBM Center.

Nomura, N., Mihashi, H. & Izumi, M. 1991. Correlation of fracture process zone and tension softening behavior in concrete. Cement and Concrete Research21: 545-550.

Zhao, Z., Kwon, S. H. & Shah, S. P. 2008. Effect of specimen size on fracture energy and softening curve of concrete: Part I. Experiments and fracture energy. Cement and Concrete Research 38(8-9): 1049-1060.